Disulfide cross-linking indicates that FlgM-bound and free σ^{28} adopt similar conformations

Margareta K. Sorenson and Seth A. Darst*

The Rockefeller University, Box 224, 1230 York Avenue, New York, NY 10021

Edited by Richard M. Losick, Harvard University, Cambridge, MA, and approved September 22, 2006 (received for review July 28, 2006)

The dissociable σ subunit of bacterial RNA polymerase is required for the promoter-specific initiation of transcription. When bound to RNA polymerase, σ makes sequence-specific promoter contacts and plays a crucial role in DNA melting. In isolation, however, σ lacks significant promoter binding activity. In the crystal structure of the flagellar σ factor, σ^{28}, bound to the anti-σ factor, FlgM, σ^{28} adopts a compact conformation in which the promoter binding surfaces are occluded by interdomain contacts. To test whether σ^{28} adopts this conformation in the absence of FlgM, we engineered a set of double cysteine mutants predicted to form interdomain disulfides in the conformation observed in the FlgM complex. We show that these disulfides form in both the presence and absence of FlgM. For two of the mutants, quantitative measurements of disulfide formation under equilibrium conditions suggest that the major solution conformation favors disulfide formation. The results indicate that the compact conformation of σ^{28} observed in the σ^{28}/FlgM structure is similar to the predominant conformation of free σ^{28} in solution. This finding suggests that autoinhibition of DNA binding in free σ^{28} is accomplished by steric occlusion of the promoter binding surfaces by interdomain interactions within the σ factor as well as by a suboptimal distance between the promoter −10 and −35 element binding determinants in σ_2 and σ_4, respectively.

protein conformation | sigma factor | transcription

In bacteria, the 450-kDa RNA polymerase (RNAP) holoenzyme, comprising the evolutionarily conserved catalytic core (subunit composition $\alpha_2\beta\beta'\omega$) combined with the initiation-specific σ subunit, directs transcription initiation (1). The σ subunit recruits RNAP to promoters through sequence-specific binding of the promoter elements and mediates formation of the transcription competent open complex. The principal control point of gene expression in bacteria is transcription initiation, and a major mechanism by which bacteria regulate transcription initiation is through regulation of σ activity.

Almost all σ's comprise a homologous family (the σ^{70} family) with defined regions of conserved amino acid sequence (2, 3). Structural analysis reveals that Group I (primary) σ's comprise four flexibly linked domains, $\sigma_{1.1}$, σ_2, σ_3, and σ_4, containing conserved regions 1.1, 1.2–2.4, 3.0–3.1, and 4.1–4.2, respectively (4). Binding to core RNAP induces large movements of the σ domains with respect to each other (5, 6), converting σ into an active conformation in which the DNA-binding determinants in σ_2 and σ_4 are exposed and appropriately spaced to recognize the −10 and −35 promoter elements, respectively (7–11). The σ's only perform their initiation activities in the RNAP holoenzyme. The structural basis for the lack of promoter binding and melting activity in free σ is not understood. To date, the structure of an intact σ in the absence of a binding partner has not been determined.

X-ray crystal structures of the flagellar σ, σ^{28}, from the motile hyperthermophile *Aquifex aeolicus* (*Aae*) in complex with its anti-σ, FlgM, explain the inhibition mechanism of FlgM (6). In the σ^{28}/FlgM complex, a previously unrecognized conformation of the σ is observed in which the structural domains, $\sigma^{28}{}_2$, $\sigma^{28}{}_3$, and $\sigma^{28}{}_4$, pack together in a compact unit. The extended FlgM wraps around the outside and occludes the core RNAP binding determinants on $\sigma^{28}{}_2$ and $\sigma^{28}{}_4$. Formation of the holoenzyme requires a helix-coil transition in the σ_3-σ_4 linker as well as large rearrangements of the σ domains with respect to each other, exposing and properly spacing the promoter binding determinants.

The extensive interdomain interactions within σ^{28} in the σ^{28}/FlgM structure suggest that this conformation may be stable in solution even in the absence of FlgM. In this inactive conformation of the σ (Fig. 1 *A* and *B*), the promoter binding determinants are buried in interdomain interfaces, preventing DNA binding, whereas the core binding surfaces, in the absence of FlgM, are exposed, allowing σ to readily interact with core RNAP, consistent with the behavior of free σ.

Here we use a disulfide cross-linking approach to investigate the solution conformation of σ^{28}. The results indicate that the compact conformation of σ^{28} observed in the σ^{28}/FlgM structure is similar to the predominant conformation of free σ^{28} in solution. This finding suggests that autoinhibition of DNA binding in free σ^{28} is accomplished by steric occlusion of the promoter binding surfaces by interdomain interactions within the σ factor as well as by a suboptimal distance between the promoter −10 and −35 element binding determinants in σ_2 and σ_4, respectively.

Results

Disulfide Mutant Design and Preparation. To investigate the conformation of free *Aae* σ^{28}, we sought to crystallize the protein in the absence of FlgM. The σ^{28} was prepared from a pET-based expression vector. Expression levels were high, and the protein was well behaved and purified to homogeneity. Nevertheless, we have been unable to obtain crystals even after extensive crystallization trials. This result did not surprise us because a free, intact σ factor has never been crystallized, despite much effort. We presume that the structural architecture of the protein, with three or four structural domains linked by flexible linkers (4, 6, 8, 9, 11–14), makes crystallization difficult. Although σ in solution likely adopts a preferred conformation (in terms of the disposition of the individual domains with respect to each other), this architecture may lead to conformational heterogeneity that is recalcitrant to crystallization.

We then considered using NMR spectroscopy to characterize the σ^{28} conformation in solution. At 27.4 kDa, σ^{28} is the smallest σ factor [excluding Group IV σ's, which lack σ_3 (14)]. Despite new technology facilitating the analysis of larger proteins (15), this target is still a challenging NMR problem. In addition, gel filtration, dynamic light scattering, and glutaraldehyde cross-

Author contributions: M.K.S. and S.A.D. designed research; M.K.S. performed research; M.K.S. analyzed data; and M.K.S. and S.A.D. wrote the paper.

The authors declare no conflict of interest.

This article is a PNAS direct submission.

Abbreviations: RNAP, RNA polymerase; *Aae*, *Aquifex aeolicus*; m1, -2, -3, and -4, mutants 1, 2, 3, and 4.

*To whom correspondence should be addressed. E-mail: darst@rockefeller.edu.

© 2006 by The National Academy of Sciences of the USA

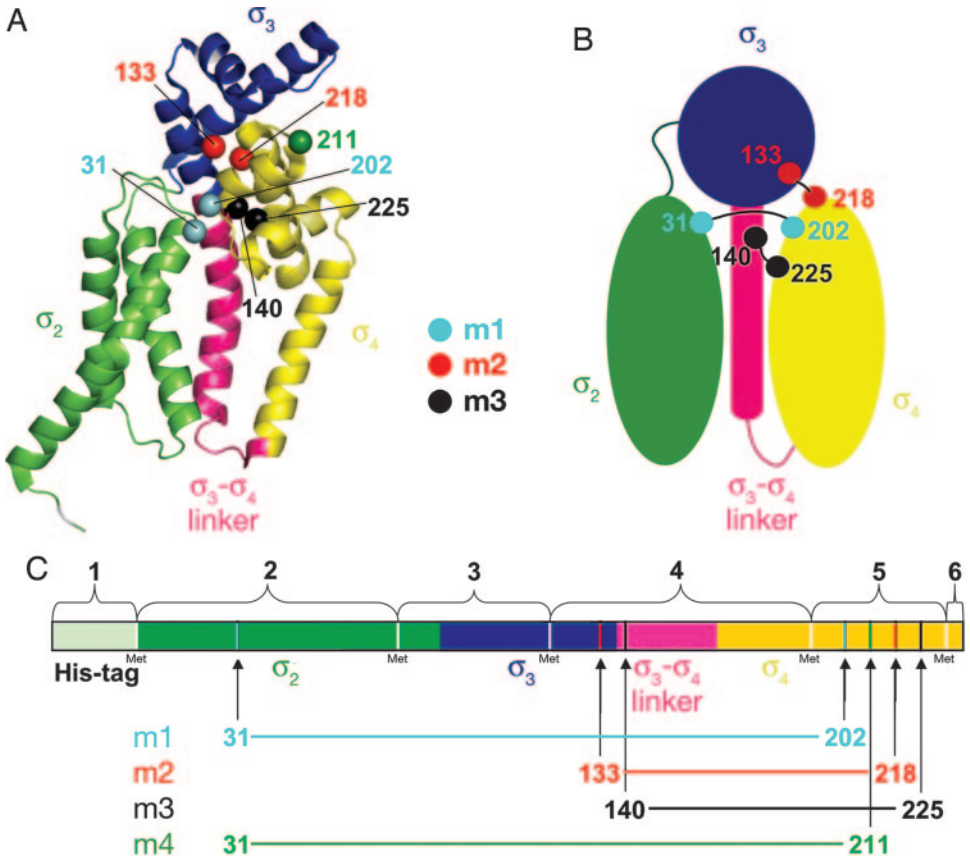

Fig. 1. Location of introduced cysteines in σ^{28}. (*A*) *Aae* σ^{28} from the σ^{28}/FlgM cocrystal structure [1RP3 (6)] is shown as a ribbon diagram. FlgM has been omitted. Structural elements are color-coded as follows: σ_2, green; σ_3, blue; σ_3-σ_4 linker, pink; and σ_4, yellow. The C^α atoms of sites mutated to cysteine are shown as spheres and color-coded as follows: m1, C31 and C202, cyan; m2, C133 and C218, red; m3, C140 and C225, black; C211 (control), green. (*B*) Schematic diagram showing the interdomain connections made by the disulfides. The color coding is the same as in *A*. (*C*) Linear representation of σ^{28}, color-coded as in *A*. The CNBr cleavage fragments are denoted by numbered brackets. Cysteine sites are indicated by vertical lines and numbered arrows (color-coded as in *A*).

linking all indicated that free σ^{28} is predominantly a dimer at high concentration, with an effective mass of ≈55 kDa, making it a very challenging target for NMR (data not shown). For this reason, we chose to pursue biochemical probes of the σ^{28} solution conformation.

Disulfide cross-linking has been used successfully as a probe of protein solution conformation and interactions (16, 17). This approach is particularly convenient in the case of *Aae* σ^{28}, because the native sequence lacks Cys residues. We analyzed the σ^{28} structure [all four copies in the asymmetric unit of the 2.3-Å-resolution structure, Protein Data Bank ID code 1RP3 (6)] with the program MODIP (18), which assesses all possible residue pairs for proximity and geometry consistent with disulfide formation (assuming the residues were mutated to Cys). Five potential interdomain disulfide pairs were identified. Two pairs were not considered further because they involved mutating an absolutely conserved residue among σ^{28} homologs (corresponding to *Aae* σ^{28} P34). This left us with three pairs of residues that, if mutated to Cys, were predicted to form interdomain disulfide bonds under appropriate conditions, provided the conformation of σ^{28} in solution (in the absence of FlgM) samples the conformation observed in the σ^{28}/FlgM complex (Fig. 1). The three pairs are as follows.

1. Mutant 1 (m1): K31/P202 (cyan in Fig. 1). This pair would form a disulfide connecting $\sigma^{28}{}_2$ with $\sigma^{28}{}_4$. Both positions are poorly conserved (in fact, *Aae* σ^{28} is the only σ^{28} with a Pro at this position).
2. Mutant 2 (m2): L133/S218 (red in Fig. 1). This pair would form a disulfide connecting $\sigma^{28}{}_3$ with $\sigma^{28}{}_4$. L133 is highly conserved. S218 is highly conserved, but mutation to a Cys would be a conservative substitution. Moreover, Cys occurs at this position in some σ^{28} homologs.
3. Mutant 3 (m3): Y140/L225 (black in Fig. 1). This pair would form a disulfide connecting the $\sigma^{28}{}_3$-$\sigma^{28}{}_4$ linker with $\sigma^{28}{}_4$. Both positions are poorly conserved.

Four double-Cys mutants of *Aae* σ^{28} were constructed beginning with a triple-Met mutant [I77M/L122M/L191M, originally constructed for phasing of the crystal structure and shown to have the same structure as the wild-type σ^{28} (6)] as the parent strain (Fig. 1*C*), to facilitate detection of disulfide bonds by CNBr cleavage (specific to peptide bonds C-terminal of Met residues). Comparison of the wild-type and σ^{28}-3M crystal structures revealed that the structure is unperturbed by the Met substitutions (6). The three mutant pairs described above, predicted to form interdomain disulfides, as well as a negative control, σ_2-31/σ_4-211 [mutant 4 (m4), green in Fig. 1], not predicted to form a disulfide in the FlgM-bound conformation, were constructed. The parent protein σ^{28}-3M and the four double-Cys mutants were each purified both in the absence and the presence of FlgM. The purifications were performed without reducing agent to allow the formation of disulfide bonds. The FlgM binding of all of the mutants was unperturbed. The only mutant that differed noticeably in its behavior from σ^{28}-3M was the negative control, σ_2-31/σ_4-211, which was toxic to the expression

host and had a tendency to form intermolecular disulfides leading to aggregation during purification.

Qualitative Identification of Disulfide Bonded Fragments by CNBr Cleavage and MALDI-TOF MS. Disulfides were detected qualitatively in m1, m2, and m3 by using CNBr cleavage and MALDI-TOF MS. The σ^{28}-3M contains five Mets, whereas FlgM lacks any internal Mets, therefore complete CNBr cleavage is predicted to yield six σ^{28}-peptide fragments (Fig. 1*C*). Because the Cys residues of each mutant pair are separated by at least one Met residue, disulfides can be detected after cleavage by MALDI-TOF MS as covalently connected CNBr fragments which disappear upon reduction.

The CNBr cleavage pattern of σ^{28}-3M was recorded as a reference, and the expected peaks were observed in the MALDI-TOF spectrum (Fig. 2*A*; For all of the MALDI-TOF experiments, the measured and expected masses for relevant fragments are listed in Table 1). In addition, a peak corresponding to CNBr cleavage products 4–5 together was observed, indicating partial cleavage at Met-191 separating CNBr fragments 4 and 5 (Fig. 2*A*). SDS/PAGE analysis of the cleavage peptides confirmed incomplete CNBr cleavage (data not shown). Modified cleavage protocols were attempted (including the addition of denaturants and addition of CNBr to saturation), but complete cleavage could not be achieved, which may be due to the presence of oxidized Mets, which are not recognized by CNBr.

The MALDI-TOF spectra of the CNBr cleavage peptides for mutant m1 in the absence (middle) and presence (bottom) of FlgM are shown in Fig. 2*A*. The peaks for the individual peptides 2 and 5 had significantly weakened signals compared with the spectrum of σ^{28}-3M (top), whereas a previously unobserved species corresponding to disulfide-linked peptides 2 and 5 (2-SS-5) appeared, confirming the formation of a C31-C202 disulfide. In addition, a disulfide bonded species containing 2 and the partially cleaved 4–5 fragment was detected [2-SS-(4–5)]. Upon reduction, the disulfide-linked peaks disappeared (data not shown), and the intensity of the individual fragments 2 and 5 increased.

The MALDI-TOF spectra of the CNBr peptides from mutant m2 without (middle) and with (bottom) FlgM are shown in Fig. 2*B*. The σ^{28}-3M CNBr spectrum is also shown as a reference (shown above *A*). A C133-C218 disulfide connects CNBr fragments 4 and 5 (4-SS-5). The mass of fragments 4 and 5 connected by a disulfide (4-SS-5) differs from that of the partially cleaved fragment (4–5) by only 16 Da, and these species are not completely resolved in the MALDI-TOF MS spectrum. The increase in the peak height for this species in the m2 spectrum compared with σ^{28}-3M is consistent with the appearance of the disulfide-linked species. Moreover, as this peak, height increases significantly, and the peak heights for the individual fragments 4 and 5 are reduced.

The expected disulfide for mutant m3 (linking C140-C255) also connects fragments 4 and 5, and the MALDI-TOF spectra for this mutant are very similar to those of m2 (data not shown). Because of the presence of intermolecular disulfides in the control mutant, m4, MALDI-TOF analysis was not expected to give an informative result.

Quantitative Disulfide Analysis by SDS/PAGE. The mobility of each disulfide mutant on a denaturing, nonreducing gel increased significantly upon disulfide formation, allowing resolution and quantitative analysis of the oxidized versus the reduced species. Each of the disulfide mutants migrated at the same rate as σ^{28}-3M when reduced (Fig. 3*A*, lanes 1–3) but showed increased mobility when oxidized (Fig. 3*A*, lanes 4 and 5), with the longest range mutant (m1) giving rise to the largest shift. For disulfide mutants m1, m2, and m3, disulfide formation under oxidizing conditions was essentially complete in the absence of FlgM (Fig. 3*A*, lane 4). The mutant m1 forms a disulfide link equally efficiently in the presence of FlgM (Fig. 3*A*, lane 5). The disulfide-bonded species predominate for both m2 and m3 in the presence of FlgM, but significant amounts of reduced protein are detectable. The negative control mutant, m4, does not form significant amounts of intramolecular disulfide under any condition, although a very faint band corresponding to this species is visible in the absence of FlgM.

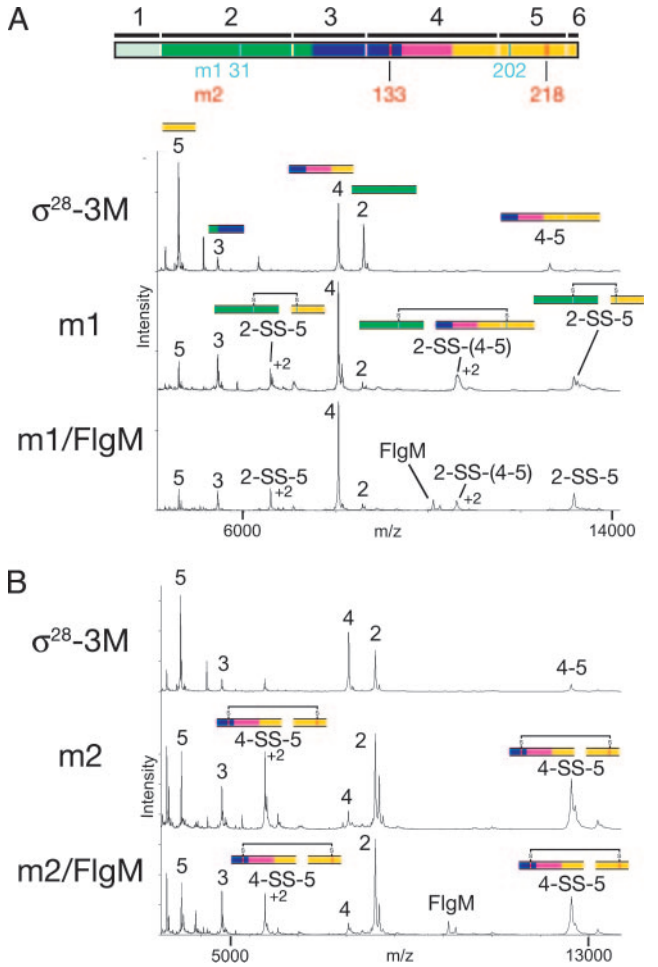

Fig. 2. MS of CNBr-digested disulfide mutants. A linear diagram of *Aae* σ^{28}, color-coded as in Fig. 1, is shown at the top of the figure. Methionines (CNBr cleavage sites) are denoted by vertical white lines, with the expected fragments from complete CNBr cleavage denoted by black bars and numbered on top. The positions of the cysteine mutants for m1 (cyan) and m2 (red) are denoted underneath the diagram. (*A*) Mass spectra of CNBr digests of σ^{28}-3M (top) and mutant m1 without (middle) and with (bottom) FlgM. Peaks are labeled with the fragment number and with colored segments corresponding to the linear diagram at the top of the figure. Peaks with charge state greater than +1 are also labeled with the charge state. (*B*) Mass spectra of CNBr digests of σ^{28}-3M (top) and mutant m2 without (middle) and with (bottom) FlgM. Peaks are labeled with the fragment number and with colored segments corresponding to the linear diagram at the top of the figure. Peaks with charge state greater than +1 are also labeled with the charge state.

Quantitative Analysis of Equilibrium Populations. Equilibrium populations of disulfide-bonded versus reduced species can be estimated by incubating the sample in buffer containing a 1:1 mixture of reduced and oxidized glutathione (19). Under these conditions, an equilibrium distribution of disulfide-bonded versus reduced species will be maintained, provided the reactive Cys residues (or S-S bond) are accessible to the glutathione in

Table 1. Observed (MALDI-TOF) and theoretical masses of CNBr fragments

Mutant	CNBr fragment no.* (residues)	Theoretical mass, Da	Observed mass, Da	|Δmass|,† Da
m1	2 (2–77)	8,574.1	8,573.3	0.8
(σ_2-31/σ_4-202)	5 (192–231)	4,588.5	4,588.3	0.2
	2-SS-5	13,160.6	13,162.0	1.4
m2	4 (123–191)	8,041.1	8,040.3	0.8
(σ_3-133/σ_4-218)	5 (192–231)	4,598.5	4,598.1	0.4
	4-SS-5	12,637.6	12,637.8	0.2
m3	4 (123–191)	7,991.1	7,990.5	0.6
(σ_{linker}-140/σ_4-225)	5 (192–231)	4,572.4	4,572.3	0.1
	4-SS-5	12,561.5	12,562.0	0.5

*See Fig. 1*C*.
†|Δmass| = |(theoretical mass) − (observed mass)|.

solution on the time scale of the experiment. The mutants were analyzed in this way, using both reduced and oxidized samples as the starting material (Fig. 3*B*). Because the same equilibrium populations should be obtained regardless of the oxidation state of the starting material, this procedure served as a control for buried sites. The mutant m1 was mostly oxidized both in the presence and absence of FlgM, and this result did not depend on the oxidation state of the starting material. Similarly, the disulfide-bonded species predominated for m2 in the absence of FlgM, both when starting with reduced protein and when starting with oxidized protein. In the presence of FlgM however, the amount of oxidation of this mutant was similar to that of the starting material, suggesting that the cysteines were inaccessible to the glutathione catalyst. The same was true for the m3 mutant with or without FlgM, and consequently this mutant was not amenable to this type of analysis. No disulfide formation was detected upon glutathione incubation in the control mutant m4.

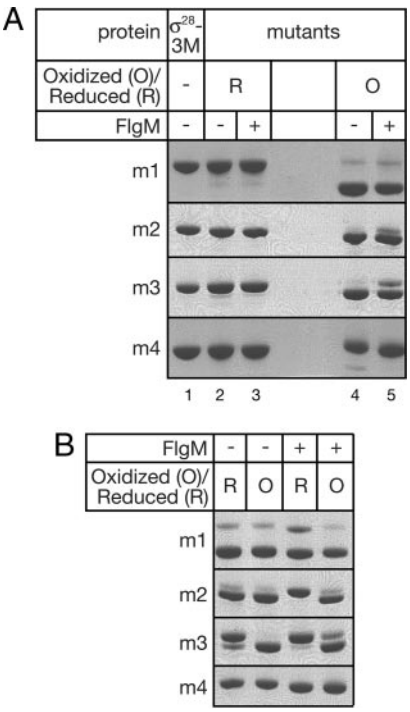

Fig. 3. SDS/PAGE analysis of disulfide mutants. Samples (oxidized or reduced as indicated) were separated on a 10% NuPAGE Novex Bistris denaturing gel. (*A*) Mobility shift of disulfide-bonded mutants (lanes 4–5) compared with the parent protein (σ^{28}-3M, which contains no cysteines, lane 1) or reduced mutants (lanes 2–3). (*B*) Analysis showing proportion of disulfide-bonded species after incubation under equilibrium conditions (see *Materials and Methods*). ''R'' indicates incubations that started with reduced samples, and ''O'' indicates incubations that started with oxidized samples.

Discussion

We have demonstrated that engineered, long-range, interdomain disulfide bridges predicted to form in σ^{28} bound to FlgM also form in free σ^{28}, indicating that the solution conformation of σ^{28} is similar to that observed in the crystal structure of the σ^{28}/FlgM complex. This conformation differs significantly from the σ^A holoenzyme structures, in which σ^A adopts an elongated conformation in which the domains are spread across one face of the enzyme, with each domain engaged with the core RNAP and with no interdomain contacts (8, 11). In the holoenzyme, the σ_3-σ_4 linker, which mostly lacks secondary structure, passes from σ_3 through the interior of the enzyme near the active site and threads out through the RNA exit channel to finally connect with σ_4. It is reasonable to assume that σ^{28} adopts a similar holoenzyme conformation, because the structures of the individual domains of *Aae* σ^{28} are very similar to the individual domains of *Taq* σ^A and because both recognize −10 and −35 promoter elements, thus requiring the same interdomain spacing. The σ_3-σ_4 linker of σ^A, however, bears no structural resemblance to the α-helical linker conformation in the σ^{28}/FlgM complex. Because detectable sequence conservation is also absent, and because a similar function has not been established for the σ_3-σ_4 linker of σ^{28} (i.e., it is not known whether the σ_3-σ_4 linker of σ^{28} passes through the RNAP active site channel like the linker of σ^A), it is not possible to predict whether the structural differences are strictly context dependent (i.e., due to binding to RNAP). However, it is reasonable to assume that σ_3 and σ_4 bind to the holoenzyme in the same manner in both σ factors. The relative positions of σ_3 and σ_4 in the holoenzyme constrain the structure of the σ_3-σ_4 linker, and modeling indicates that the helical conformation found in the σ^{28}/FlgM complex is incompatible with holoenzyme formation.

We have directly shown that σ_2 and σ_4 can be disulfide-linked in free σ^{28}, and equilibrium measurements suggest that this represents a favored conformation. The maximum distance between the C^α atoms of two cysteines to form a disulfide is 7 Å (20), and in the σ^{28}/FlgM complex, the C^α atoms of R31 and P202 are 5.36 Å apart. In the *Taq* holoenzyme (8), the corresponding residues of σ^A, G219 and T397, are 63.26 Å apart, appropriately spaced for −10 and −35 recognition (Table 2). The close proximity of these domains in free σ^{28} is thus incompatible with simultaneous recognition of these promoter elements, providing one explanation for autoinhibition and suggesting that these residues should move apart by ≈58 Å upon binding to core RNAP. A study using luminescence resonance energy transfer between introduced probes has shown that the

BIOCHEMISTRY

Table 2. Distances (C^{α}–C^{α}) between σ^{28} residue pairs in the FlgM- and holoenzyme-bound conformations

Residue pair		C^{α}–C^{α} distance, Å	
Aae σ^{28}	*Taq* σ^{A}	*Aae* σ^{28}/FlgM (ref. 6)	*Taq* σ^{A}-holoenzyme (ref. 7)
K31/P202 (m1)	G219/T397	5.36	63.26
L133/S218 (m2)	L323/R413	6.56	57.08
Y140/L225 (m3)	V330/L420	5.93	51.21

distance between σ_2 and σ_4 increases by 15 Å in *Escherichia coli* σ^{70} upon holoenzyme formation (5). Although qualitatively this is consistent with our results, our data suggest a much greater magnitude. Alternatively, the average distance between these domains in free σ may be greater than that trapped by the disulfide, giving rise to a smaller net movement upon binding to core, but the equilibrium measurements argue against this. Another possibility is that the conformation of *Escherichia coli* σ^{70} is altogether different from that of σ^{28}. Comparison of the C^{α}–C^{α} distances between the *Taq* σ^{A} residues corresponding to the other two disulfide pairs (m2 and m3) with those in the σ^{28}/FlgM complex also reveals large differences in the two conformations (Table 2).

We have also shown that σ_3 and σ_4 can be disulfide-linked in the m2 mutant and that this disulfide is favored at equilibrium in free σ^{28}. The larger proportion of disulfide bonded species in free σ^{28} (compared with the FlgM complex) indicates that disulfide formation in this mutant is more rapid in the absence of FlgM (Fig. 3). This observation suggests that the proximity of the domains is similar but that rigidity imposed by FlgM decreases the rate of disulfide formation. Under equilibrium conditions, mostly oxidized protein was obtained for free σ^{28}, regardless of whether the protein was reduced or oxidized at the beginning of the experiment (Fig. 3*B*). For the FlgM-bound species, in contrast, the population after incubation under equilibrium conditions resembled the starting material, suggesting that the site was inaccessible to the catalyst. FlgM does not directly occlude this site in the structure, but it may constrain interdomain flexibility which otherwise would allow access of the catalyst. S218 of *Aae* σ^{28} corresponds to R413 of *Taq* σ^{A}, which has been observed in a cocrystal structure to interact with the −35 element (4). Although the −35 binding surface of σ^{28} has not been established, it is reasonable to infer that σ^{28} binds to the −35 element using the same surface of σ_4. Interaction with L133 of σ_3 thus buries the −35 binding surface, directly occluding it, and providing a role for σ_3 in autoinhibition of promoter binding. L133 is located on an acidic face of σ_3, and the acidity of this surface is conserved in Group I σ factors, as noted in ref. 6. Thus, this mode of autoinhibition may be more general.

In Group I σ's, the N-terminal region 1.1 ($\sigma_{1.1}$) contributes to the autoinhibition mechanism, because σ's with N-terminal truncations of $\sigma_{1.1}$ show detectable, promoter-specific binding (21, 22). The autoinhibition was proposed to occur through a direct interaction between $\sigma_{1.1}$ and conserved region 4.2 that would occlude the −35 element recognition determinants in region 4.2 (21). However, NMR studies (22) ruled out a direct $\sigma_{1.1}/\sigma_{4.2}$ interaction, indicating that $\sigma_{1.1}$ acts indirectly to inhibit promoter binding. Our finding reported here lead us to suggest that in Group I σ's, $\sigma_{1.1}$ may act indirectly to inhibit promoter binding by stabilizing a compact conformation of σ that is incompatible with promoter recognition.

Finally, we have demonstrated by using mutant m3 that a cysteine introduced into the σ_3-σ_4 linker cross-links to a cysteine in the C-terminal helix of σ_4, both in the FlgM complex and in free σ^{28}. In the σ^{A}-holoenzyme, the corresponding part of the linker is unfolded. Because the cross-link requires this residue to be on the appropriate side of the linker helix, its formation supports the idea that the σ_3-σ_4 linker is α-helical even in free σ^{28}. The disulfide formation was more rapid in free σ^{28} than in the FlgM/σ^{28} complex for mutant m3 as well, again suggesting greater flexibility but a similar conformation of free σ^{28}.

Together these data suggest that the conformation of free σ^{28} resembles that observed in the FlgM complex but that it is less rigid. This conformation provides an explanation for the autoinhibition of DNA binding and provides insight into the conformational change that accompanies binding to core RNAP. Autoinhibition is accomplished both by suboptimal interdomain distances and by steric occlusion of both promoter element binding surfaces. We suggest that these principles of σ factor regulation may apply to Group I σ factors as well.

Materials and Methods

Mutagenesis. The program MODIP (18) provided a list of pairs of residues which, if mutated to cysteine, are predicted to form disulfides, based on the crystal structure of *Aae* σ^{28}/FlgM (Protein Data Bank ID code 1RP3). Four double cysteine mutants of *Aae* σ^{28} were constructed in a triple methionine mutant I77M/L122M/L191M (σ^{28}-3M) background. The cysteine mutations were introduced by site-directed mutagenesis, giving the quintuple mutants: m1, σ^{28}-3M/R31C/P202C (σ_2-31/σ_4-202); m2, σ^{28}-3M/R31C/E211C (σ_2-31/σ_4-211); m3, σ^{28}-3/L133C/S218C (σ_3-133/σ_4-218); and the negative control m4, σ^{28}-3M/Y140C/L225C (σ_{linker}-140/σ_4-225). The correct DNA sequence was confirmed for each construct.

Expression and Purification. σ^{28}-3M and each of the four disulfide mutants were expressed in BL21-CodonPlus (DE3)-RIL (Stratagene, La Jolla, CA) except for m4, which was expressed in 4L Rosetta (DE3)pLysS (Novagen, San Diego, CA). The cells were grown in LB with shaking at 37°C. At OD_{600} of 0.4–0.6 expression was induced by adding 1 mM isopropyl β-D-thiogalactoside, and the temperature was lowered to 19°C. The cells were harvested by centrifugation after 14–16 h. *Aae* FlgM in pET21a (without any tag) was expressed separately in the same way. The pellets were resuspended in 20 mM Tris·HCl (pH 8.0), 0.5 M NaCl, and a protease inhibitor mixture (final concentration of protease inhibitors of 174 μg/ml PMSF, 312 μg/ml benzamidine, 5 μg/ml chymostatin, 5 μg/ml leupeptin, 1 μg/ml pepstatin, and 10 μg/ml aprotinin). The cells were lysed with a French press, and the soluble fraction was removed by centrifugation. One-half of the soluble lysate of each mutant was mixed with soluble FlgM lysate (corresponding to 2L culture), and the other half was kept separate. The lysates were then incubated at 65°C for 45 min to precipitate heat-sensitive *Escherichia coli* proteins. Precipitated contaminants were removed by centrifugation, and the soluble protein was purified by using Ni^{2+}-chelating chromatography. For the FlgM complexes, this step removes excess FlgM, yielding a 1:1 σ^{28}/FlgM complex. The Ni^{2+} eluates were further purified on a Superdex 75 (GE Healthcare, Piscataway, NJ) gel filtration column in 20 mM Tris·HCl (pH 8.0) and 0.5 M NaCl. The pure protein was concentrated to between 8 and 70 mg/ml in the same buffer. No reducing agent was added at any time during the purification, and disulfides formed during purification without the aid of a catalyst.

CNBr Cleavage and MALDI-TOF MS. CNBr crystals were dissolved in 20 μl of 1 mg/ml protein in 70% TFA and then incubated for 19 h in the dark at room temperature. The samples were subsequently dried in a SpeedVac (Savant, Irvine, CA) and redissolved in 20 μl of water. For MALDI-TOF MS, the samples were first diluted to 1 mg/ml in 67% acetonitrile and 0.1% TFA and then diluted to 0.2 mg/ml in the same solvent saturated with α-cyano-4-hydroxycinnamic acid and immediately spotted on a MALDI sample plate as described (23).

SDS/PAGE Analysis. Concentrated protein stock was diluted in 20 mM Tris·HCl (pH 8.0) and 0.5 M NaCl to 0.25–0.5 mg/ml. The protein was then mixed 4:1 with 5× SDS sample buffer (with or without β-mercaptoethanol, as noted), then heated to ≈100°C for 1 min before loading. NuPAGE 10% Bistris precast gels (Invitrogen, Carlsbad, CA) were used with Mops running buffer (50 mM Mops, 50 mM Tris base, 0.1% SDS, 1 mM EDTA, pH 7.7). The gels were run at 200 V for 1–2 h and stained with Coomassie brilliant blue.

Glutathione Catalyzed Disulfide Equilibrium Measurements. The procedure was essentially as described in ref. 19. Concentrated protein was diluted to 1 mg/ml in 20 mM Tris (pH 8), 0.5 M NaCl, and 100 mM DTT and incubated at 37°C for 90 min. Fifty microliters of reduced protein was then dialyzed against >1 L of 10 mM Tris (pH 7.5), 0.5 M NaCl, and 0.1 mM EDTA for 4 h with a buffer change after 2 h, at 4°C. Ten microliters of dialyzed protein was removed and alkylated by adding 2.5 μl of 50 mM iodoacetamide and incubated for 1 h in the dark at room temperature. Twenty microliters of the remaining protein was mixed with 5 μl of 250 mM Tris·HCl (pH 9.0), 0.5 M NaCl, and 2.5 mM reduced glutathione and 2.5 mM oxidized glutathione and incubated for 16 h at room temperature, and then alkylated with iodoacetamide as described above.

We thank B. T. Chait (Laboratory of Mass Spectrometry and Gaseous Ion Chemistry, The Rockefeller University) for access to MS facilities and Soumya S. Ray for helpful discussions. This work was supported by a National Science Foundation Graduate Research Fellowship (to M.K.S.) and National Institutes of Health Grant GM53759 (to S.A.D.).

1. Gross CA, Chan C, Dombroski A, Gruber T, Sharp M, Tupy J, Young B (1998) *Cold Spring Harbor Symp Quant Biol* 63:141–155.
2. Gruber TM, Bryant DA (1997) *J Bacteriol* 179:1734–1747.
3. Lonetto M, Gribskov M, Gross CA (1992) *J Bacteriol* 174:3843–3849.
4. Campbell EA, Muzzin O, Chlenov M, Sun JL, Olson CA, Weinman O, Trester-Zedlitz ML, Darst SA (2002) *Mol Cell* 9:527–539.
5. Callaci S, Heyduk E, Heyduk T (1999) *Mol Cell* 3:229–238.
6. Sorenson MK, Ray SS, Darst SA (2004) *Mol Cell* 14:127–138.
7. Kuznedelov K, Minakhin L, Niedziela-Majka A, Dove SL, Rogulja D, Nickels BE, Hochschild A, Heyduk T, Severinov K (2002) *Science* 295:855–857.
8. Murakami K, Masuda S, Darst SA (2002) *Science* 296:1280–1284.
9. Murakami K, Masuda S, Campbell EA, Muzzin O, Darst SA (2002) *Science* 296:1285–1290.
10. Murakami K, Darst SA (2003) *Curr Opin Struct Biol* 13:31–39.
11. Vassylyev DG, Sekine S, Laptenko O, Lee J, Vassylyeva MN, Borukhov S, Yokoyama S (2002) *Nature* 417:712–719.
12. Malhotra A, Severinova E, Darst SA (1996) *Cell* 87:127–136.
13. Campbell EA, Masuda S, Sun JL, Muzzin O, Olson CA, Wang S, Darst SA (2002) *Cell* 108:795–807.
14. Campbell EA, Tupy JL, Gruber TM, Wang S, Sharp MM, Gross CA, Darst SA (2003) *Mol Cell* 11:1067–1078.
15. Pervushin K, Riek R, Wider G, Wuthrich K (1997) *Proc Natl Acad Sci USA* 94:12366–12371.
16. Anthony LC, Burgess RR (2002) *J Biol Chem* 277:46433–46441.
17. Anthony LC, Dombkowski AA, Burgess RR (2002) *J Bacteriol* 184:2634–2641.
18. Sowdhamini R, Srinivasan N, Shoichet B, Santi DV, Ramakrishnan C, Balaram P (1989) *Protein Eng* 3:95–103.
19. Dorigo B, Schalch T, Kulangara A, Duda S, Schroeder RR, Richmond TJ (2004) *Science* 306:1571–1573.
20. Dani VS, Ramakrishnan C, Varadarajan R (2003) *Protein Eng* 16:187–193.
21. Dombroski AJ, Walter WA, Record MT, Siegele DA, Gross CA (1992) *Cell* 70:501–512.
22. Camarero JA, Shekhtman A, Campbell EA, Chlenov M, Gruber TM, Bryant DA, Darst SA, Cowburn D, Muir TW (2001) *Proc Natl Acad Sci USA* 99:8536–8541.
23. Cadene M, Chait BT (2000) *Anal Chem* 72:5655–5658.